Inverse homogenization design of lattice structures without scale separation

Daicong Da

Version of Record: https://www.sciencedirect.com/science/article/pii/S2352012420306640
Manuscript_d574596eb8314c0a6480dec89f15fc13

Inverse homogenization design of lattice structures without scale separation

Daicong Da[a,*]

[a]*Université Paris-Est, MSME, UMR CNRS 8208, 5 bd Descartes, 77454 Marne-la-Vallée, France*

Abstract

Scale separation is often assumed in most homogenization-based topology optimization (TO) frameworks for design of material microstructures. This work goes beyond the mainstream TO contributions by abandoning the scale separation hypothesis. First, we put to evidence the limits of the homogenization-based approach when the size of the Representative Volume Element (RVE) is not negligible with respect to the structure. Then, a re-localized scheme bridging the RVE and the structure is proposed to reproduce the microscopic fields, while the structure problem at the macroscopic scale is solved only based on the coarse mesh. Finally, we show interesting results on 2D lattice structures within the proposed framework giving a hint towards a feasible realization of the finite-scale lattice structures with current resolution of additive manufacturing technologies. Numerical experiments evidence that the present method can lead to the same topology and stiffness of the optimized structures as the reference solution when the number of unit cell is relatively large, while reducing the computational costs significantly.

Keywords: Homogenization, Structural optimization, Scale separation, Representative Volume Element, relocalization, Stiffness

1. Introduction

The homogenization method [1] has been widely used to predict the effective macroscopic properties of heterogeneous materials with periodic microstructures such as fiber-reinforced composites. Scale separation is one of the central assumptions. It is stated that the characteristic length of the microstructural details are much smaller than the dimensions of the whole structure, or that the characteristic wavelength of the applied load is much larger than that of the local fluctuation of mechanical fields. On the other hand, the material properties depend on not only its constituent/component phases but also the morphology of its microstructures. Combined with the topology optimization strategy [2], the material microstructures had been tailored to obtain specific elastic modulus [3]. This scheme has been extensively extended to design for many other material properties [4–6] or even exotic/meta- materials [7–10]. Apart from material properties, the design of

*Corresponding author
Email address: daicong.da@univ-paris-est.fr (Daicong Da)

material microstructures has also been extended for considering specific macrostructural performance, e.g. stiffness, nature frequency etc. However, in all these works, the assumption of scale separation is often assumed when classical homogenization method is used to link the material microstructural geometries and macroscopic properties. By this way, the designed microstructures have no distinct geometrical dimension, and it is thus cannot be manufactured even by current additive manufacturing technologies.

To reveal the effectiveness of the homogenization method when the scales are not separated, size effect of the periodic unit cell has been investigated. Differences between the direct FE discretization method, the homogenization method and the classical beam theory have been compared in [11]. It is concluded that the homogenized solution is the limit value whenever the scale factor tends to be infinitely large. As for the material design problem, the effective material properties given by homogenization may be inaccurate when the scaling requirement is not meet, leading to error in the material design process, as stated in [12]. It is then suggested that other tools, e.g. averaging method, should be provided to link the two scales to overcome some of these limitations. Recently, size effect analysis of optimized microstructures by the inverse homogenization method has been provided in [13], which elucidates that periodic homogenization method could be mechanically admissible to predict the equivalent moduli even with small number of unit cell repetitions. However, to our best knowledge, size effect analysis of the periodic unit cell in the topology optimization through the homogenization approach for specific structural response has not been investigated yet.

In the present work, the objective is to develop a topology optimization procedure based on the classical homogenization method for periodic structures in a context of non-separated scales. The dimensions of the unit cell will range from large to small as compared with the dimensions of the whole structure to highlight the size effect. Particularly, a relocalization scheme is proposed based on the computational homogenization method served a link between two scale fields, allowing performing the topological optimization problem on a coarse mesh. Corresponding reference solution is obtained by fully meshing the heterogeneities in whole structures as a comparison. The present paper then tries to answer the question that how good the homogenization method-based topology optimization for periodic structures with the size of the periodic cell changing from large to small, comparing the characteristic length of the whole structure. To our best knowledge, in the context of non-separated scale, topology optimization combined with the classical homogenization scheme for periodic structures design is investigated here for the first time.

The remainder of the paper is organized as follows. The classical homogenization technique is reviewed in section 2. Details of numerical computation of effective material properties as well as the relocalization scheme are provided. Presented topological optimization model and method are given in section 3. Bi-directional evolutionary structural optimization (BESO) method is adopted to perform the topology optimization due to the simplicity. Numerical experiments are conducted in section 4 to fully investigate the size effect of the periodic unit cells and answer the question that when the optimized cells could be effective for real structural stiffness performance. Finally, the conclusion is given in section 5.

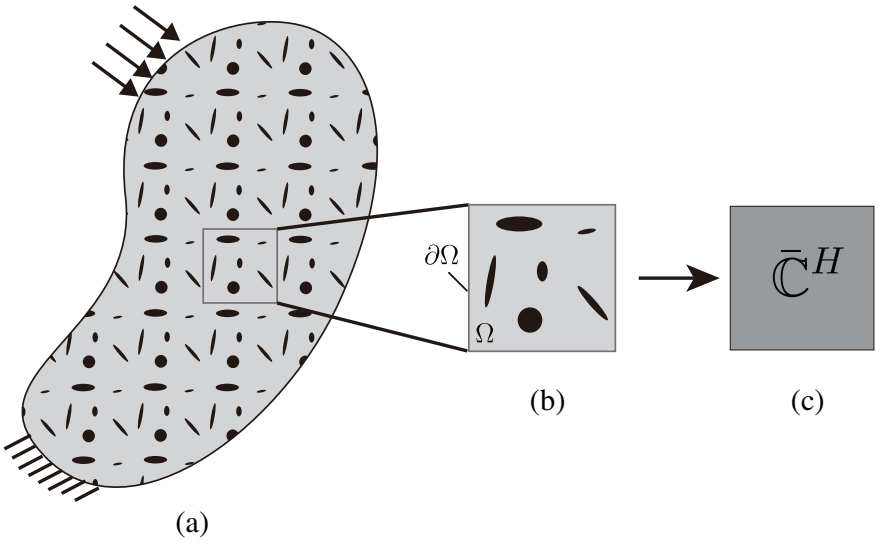

Figure 1: Illustration of a heterogeneous structure composed of periodic unit cells: (a) heterogeneous structure; (b) RVE; (c) homogenized material.

2. The classical homogenization method

In this section, the computation of effective or homogenized material properties of heterogeneous composite in the context of linear elasticity is reviewed. The local problem at microscopic scale with different types of boundary conditions is firstly introduced, followed by the numerical implementation to evaluate the effective elastic matrix by means of the classical finite element method (FEM).

2.1. Localization problem

A heterogeneous structure composed of two-phase composite is considered here as described in Figure 1 (a). The RVE shown in Figure 1 (b) is associated with a domain Ω and boundary $\partial\Omega$. The objective is to define the effective or homogenized elastic tensor $\bar{\mathbb{C}}^H$. The constitutive material phases are assumed isotropic with constant elastic properties, and the interfaces between the different constitutive phases are assumed to be perfect. Therefore, the local problem assuming that the RVE is subject to homogeneous strains is formulated as follows. Applying a constant macroscopic strain $\bar{\boldsymbol{\varepsilon}}$, find the displacement field $\boldsymbol{\mu}(\boldsymbol{x})$ in Ω satisfying:

$$\nabla \cdot (\boldsymbol{\sigma}(\boldsymbol{x})) = 0 \quad \text{in } \Omega \tag{1}$$

and

$$\boldsymbol{\sigma}(\boldsymbol{x}) = \mathbb{C}(\boldsymbol{x}) : \boldsymbol{\varepsilon}(\boldsymbol{x}) \tag{2}$$

with

$$\langle \boldsymbol{\varepsilon} \rangle = \bar{\boldsymbol{\varepsilon}} \quad \text{in } \Omega \tag{3}$$

where $\mathbb{C}(\boldsymbol{x})$ is the constant fourth-order elasticity tensor associated with different phases, $\nabla \cdot (\cdot)$ denotes the divergence operator, and $\langle \cdot \rangle$ denotes the space averaging over Ω. Following [14], the

split of local strain field into a constant macroscopic strain field $\bar{\boldsymbol{\varepsilon}}$ and a remaining local fluctuation $\tilde{\boldsymbol{\varepsilon}}$ is assumed:

$$\boldsymbol{\varepsilon}(\boldsymbol{x}) = \bar{\boldsymbol{\varepsilon}}(\boldsymbol{x}) + \tilde{\boldsymbol{\varepsilon}}(\boldsymbol{x}) \tag{4}$$

Taking average of the above equation, we have

$$\langle \boldsymbol{\varepsilon}(\boldsymbol{x}) \rangle = \bar{\boldsymbol{\varepsilon}} + \langle \tilde{\boldsymbol{\varepsilon}}(\boldsymbol{x}) \rangle = \bar{\boldsymbol{\varepsilon}} + \frac{1}{|\Omega|} \int_{\Omega} \tilde{\boldsymbol{\varepsilon}}(\boldsymbol{x}) d\Omega = \bar{\boldsymbol{\varepsilon}} + \frac{1}{2|\Omega|} \int_{\Omega} \{\nabla(\tilde{\boldsymbol{u}}(x)) + \nabla^T(\tilde{\boldsymbol{u}}(x))\} d\Omega \tag{5}$$

where $\tilde{\boldsymbol{u}}$ is the unknown fluctuation displacement as $\tilde{\boldsymbol{u}} = \boldsymbol{u}(\boldsymbol{x}) - \bar{\boldsymbol{\varepsilon}}\boldsymbol{x}$. Using the divergence theorem, we have

$$\langle \boldsymbol{\varepsilon}(\boldsymbol{x}) \rangle - \bar{\boldsymbol{\varepsilon}} = \frac{1}{2|\Omega|} \int_{\partial\Omega} \{\tilde{\boldsymbol{u}}(x) \otimes \mathbf{n} + \mathbf{n} \otimes (\tilde{\boldsymbol{u}}(x)\} d\Gamma \tag{6}$$

Note that the condition (3) can be satisfied by solving the present local problem Equations (1)-(2) with appropriate boundary conditions. In other words, the right-hand side of Equation (6) should be equal to zero. It can be verified with the following two possible conditions:

$$\tilde{\boldsymbol{u}}(\boldsymbol{x}) = 0 \ \text{ on } \partial\Omega \quad \text{or} \quad \tilde{\boldsymbol{u}}(\boldsymbol{x}) \ \text{ is periodic on } \partial\Omega \tag{7}$$

Following [14], the corresponding two types of boundary conditions can be obtained by integrating Equation (4) with respect to $\boldsymbol{x}$. The first is called Kinematically Uniform Boundary Conditions (KUBC) and is expressed as

$$\boldsymbol{u}(\boldsymbol{x}) = \bar{\boldsymbol{\varepsilon}}\boldsymbol{x}, \forall \boldsymbol{x} \in \partial\Omega \tag{8}$$

where the displacement is imposed directly at boundary points. In the second type of boundary conditions which is named Periodic Boundary Condition (PER), the displacement field over the boundary $\partial\Omega$ takes the form

$$\boldsymbol{u}(\boldsymbol{x}) = \bar{\boldsymbol{\varepsilon}}\boldsymbol{x} + \tilde{\boldsymbol{u}}, \forall \boldsymbol{x} \in \partial\Omega \tag{9}$$

where the fluctuation term $\tilde{\boldsymbol{u}}(\boldsymbol{x})$ is periodic on $\partial\Omega$, i.e. it takes the same values on two points of opposite faces over $\partial\Omega$. It should be mentioned that an alternative localization problem assuming that the RVE is subjected to a constant stress field can also be used to predict the effective material properties. For detailed information about stress averaging theorem as well as the corresponding boundary conditions one can refer to [14]. In this work, the second type of boundary conditions is adopted to solve the present localization problem. It is also worth noting that even though only two-phase RVE are considered here, the procedure can be straightforwardly extended to an arbitrary number of phases.

2.2. Definition and computation of the effective material properties

With the superposition principle, the solution of the local problem in Equations (1)-(2) can be viewed as a linear combination of 3 independent components of the strain tensor in 2D:

$$\boldsymbol{u}(\boldsymbol{x}) = \boldsymbol{u}^{(11)}(\boldsymbol{x})\bar{\varepsilon}_{11} + \boldsymbol{u}^{(22)}(\boldsymbol{x})\bar{\varepsilon}_{22} + 2\boldsymbol{u}^{(12)}(\boldsymbol{x})\bar{\varepsilon}_{12} \tag{10}$$

where $\boldsymbol{u}^{(ij)}(\boldsymbol{x})$ is the displacement field obtained by solving the local problem (Equations (1)-(2)) together with the PER (Equation (9)) using

$$\bar{\boldsymbol{\varepsilon}} = \frac{1}{2}(e_i \otimes e_j + e_j \otimes e_i) \tag{11}$$

where e_i ($i = 1, 2$) are unitary basis vectors. To be specific, $\boldsymbol{u}^{(11)}$, $\boldsymbol{u}^{(22)}$ and $\boldsymbol{u}^{(12)}$ are respectively obtained by solving the local problem with

$$\bar{\varepsilon} = \begin{bmatrix} 1 & 0 \\ 0 & 0 \end{bmatrix}, \quad \bar{\varepsilon} = \begin{bmatrix} 0 & 0 \\ 0 & 1 \end{bmatrix}, \quad \bar{\varepsilon} = \begin{bmatrix} 0 & 1/2 \\ 1/2 & 0 \end{bmatrix} \tag{12}$$

Setting $\boldsymbol{\varepsilon}^{(ij)}(\boldsymbol{x}) = \varepsilon(\boldsymbol{u}^{(ij)}(\boldsymbol{x}))$, we have:

$$\varepsilon(\boldsymbol{x}) = \boldsymbol{\varepsilon}^{(11)}(\boldsymbol{x})\bar{\varepsilon}_{11} + \boldsymbol{\varepsilon}^{(22)}(\boldsymbol{x})\bar{\varepsilon}_{22} + 2\boldsymbol{\varepsilon}^{(12)}(\boldsymbol{x})\bar{\varepsilon}_{12} \tag{13}$$

This expression can be re-written in a compact form as

$$\boldsymbol{\varepsilon}(\boldsymbol{x}) = \mathbb{A}(\boldsymbol{x}) : \bar{\boldsymbol{\varepsilon}}, \quad \forall \boldsymbol{x} \in \Omega \tag{14}$$

where $\mathbb{A}(\boldsymbol{x})$ is the fourth-order localization tensor relating microscopic and macroscopic strains with

$$A_{ijkl}(\boldsymbol{x}) = \varepsilon_{ij}^{(kl)}(\boldsymbol{x}) \tag{15}$$

Using the classical Hooke's law, we have

$$\sigma_{pq}(\boldsymbol{x}) = C_{pqij}(\boldsymbol{x})A_{ijkl}(\boldsymbol{x})\bar{\varepsilon}_{(kl)} \tag{16}$$

or

$$\boldsymbol{\sigma}(\boldsymbol{x}) = \mathbb{C}(\boldsymbol{x}) : \mathbb{A}_{ijkl}(\boldsymbol{x}) : \bar{\boldsymbol{\varepsilon}} \tag{17}$$

By taking the spatial average over Ω, the constitutive relationship at macroscopic scale can be formulated as:

$$\bar{\boldsymbol{\sigma}} = \bar{\mathbb{C}}^H : \bar{\boldsymbol{\varepsilon}} \tag{18}$$

with

$$\bar{\mathbb{C}}^H = \langle \mathbb{C}(\boldsymbol{x}) : \mathbb{A}(\boldsymbol{x}) \rangle \tag{19}$$

Using classical displacement-based FEM, a matrix $\boldsymbol{U}$ containing in each row the nodal displacement solution of the above 3 local problems in one element is defined. Therefore, the matrix form of the localization tensor $\mathbb{A}$ in Equation (14) or (15) can be written as

$$\boldsymbol{A}(\boldsymbol{x}) = \boldsymbol{B}(\boldsymbol{x})\boldsymbol{U} \tag{20}$$

where $\boldsymbol{B}$ is the strain matrix. The matrix form of the effective elasticity tensor $\bar{\mathbb{C}}^H$ in Equation (19) is then given by:

$$\bar{\boldsymbol{C}}^H = \frac{1}{V}\int_\Omega \boldsymbol{C}(\boldsymbol{x})\boldsymbol{B}(\boldsymbol{x})\boldsymbol{U}d\Omega \tag{21}$$

2.3. Numerical implementation for the local problem with PER

Following [14], a technique based on Lagrange multipliers to enforce the PER in 2D cases is presented here. From Equation 9, the displacement on the opposite faces of the RVE is expressed as

$$\begin{cases} u_i^{k+} = \bar{\varepsilon}_{ij} x_j^{k+} + \tilde{u}_i^* \\ u_i^{k-} = \bar{\varepsilon}_{ij} x_j^{k-} + \tilde{u}_i^* \end{cases} \tag{22}$$

where superscripts "$k+$" and "$k-$" denote nodes on the pair of opposite surfaces of the cell. $\tilde{u}_i^*$ is the periodic fluctuation field which can be eliminated by comparing the difference between the displacements:

$$u_i^{k+} - u_i^{k-} = \bar{\varepsilon}_{ij}(x_j^{k+} - x_j^{k-}) = R^{k+k-} \tag{23}$$

Therefore, in order to enforce the periodic boundary conditions using the Lagrange multipliers method, the constraint equations can be written as following:

$$\boldsymbol{P}\boldsymbol{u} - \boldsymbol{R} = 0 \tag{24}$$

The discrete form is written as

$$C_i^{k+k-} = P_{ij} u_j - R_i^{k+k-} = 0 \tag{25}$$

where $\boldsymbol{P}$ is a matrix relating the whole indices of coupled nodes on opposite faces of the RVE, which is completely filled with the numbers 1, 0 and -1. It is noted that there are two constraint equations for each pair of nodes on the boundaries in the case here. The constrained minimization problem then can be stated as

$$\inf_{\substack{\boldsymbol{u} \\ C_i=0,\ i=1,\dots,n_c}} \frac{1}{2}\boldsymbol{u}^T \boldsymbol{K}\boldsymbol{u} \tag{26}$$

where $\boldsymbol{u}$ is the global vector of required displacement, and n_c is the number of constraint equations. Introducing the vector of Lagrange multipliers Λ associated with the adopted periodicity constraints, the above equation can be re-written as

$$\mathcal{L} = \frac{1}{2}\boldsymbol{u}^T \boldsymbol{K}\boldsymbol{u} + \Lambda \cdot (\boldsymbol{P}\boldsymbol{u} - \boldsymbol{R}) \tag{27}$$

The stationary of $\mathcal{L}$ is found by

$$\begin{cases} D_{\delta \boldsymbol{u}} \mathcal{L} = 0 \\ D_{\delta \Lambda} \mathcal{L} = 0 \end{cases} \tag{28}$$

Therefore, we have:

$$\begin{cases} \delta \boldsymbol{u}^T \boldsymbol{K}\boldsymbol{u} + \Lambda \cdot \boldsymbol{P}\delta \boldsymbol{u} = 0 \\ \delta \Lambda^T \boldsymbol{P}\boldsymbol{u} = \delta \Lambda^T \boldsymbol{R} \end{cases} \tag{29}$$

Since the arbitrariness of $\delta \boldsymbol{u}$ and $\delta\Lambda$, the following linear system can be obtained:

$$\begin{bmatrix} \boldsymbol{K} & \boldsymbol{P}^T \\ \boldsymbol{P} & 0 \end{bmatrix} \begin{bmatrix} \boldsymbol{u} \\ \Lambda \end{bmatrix} = \begin{bmatrix} 0 \\ \boldsymbol{R} \end{bmatrix} \tag{30}$$

where $\boldsymbol{K}$ is the global stiffness matrix after discretizing the elastic problem (1) without enforcing the Dirichlet boundary conditions, and the vector $\boldsymbol{R}$ can be trivially obtained through Equation (23).

3. Topology optimization model and procedure

3.1. Optimization model and sensitivity number

In this work, the macroscopic structure is assumed to be composed of microscopic substructures/RVEs periodically. Effective material properties of the considered heterogeneous microstructures are calculated based on the above formulated homogenization method, even though the length scale of the microscopic RVE is comparable to the higher scale structures. The topology of the RVE is tailored by means of topology optimization such that the obtained structure has the optimal stiffness with certain amount of materials. The final goal is to investigate the size effect of the RVE when micro and macro scales are clearly non-separated. Therefore, this work aims to answer the following question: When the ratio between the size of the RVE and the size of the real macrostructure is used, the classical homogenization method can be used as an effective tool for multiscale topology optimization of periodic structures without scale separation. This topology optimization problem can be stated mathematically as follows:

$$\text{Find} : \{\boldsymbol{\rho}^{(1)}, \ldots, \boldsymbol{\rho}^{(N_s)}\} \tag{31}$$

$$\text{Minimize} : f_c(\boldsymbol{\rho}, \bar{\mathbf{u}}) = \bar{\mathbf{F}}^T \bar{\mathbf{u}} \tag{32}$$

$$\text{Subject to} : \bar{\mathbf{K}}\bar{\mathbf{u}} = \bar{\mathbf{F}} \tag{33}$$

$$: V(\boldsymbol{\rho}) = \sum \rho_e^{(k)} v_e^{(k)} = V_{\text{req}},\ k = 1, \ldots, N_s \tag{34}$$

$$: \rho_e^{(1)} = \cdots = \rho_e^{N_\text{s}},\ e = 1, \ldots, N_e \tag{35}$$

$$: \rho_e^{(k)} = \rho_{min} \text{ or } 1,\ e = 1, \ldots, N_\text{e},\ k = 1, \ldots, N_s \tag{36}$$

where f_c is the objective function of macrostructural compliance. $\bar{\mathbf{F}}$ and $\bar{\mathbf{u}}$ are the global load and displacement vectors, respectively. V_{req} is the required/prescribed volume of solid material in each RVE. N_s is the number of the periodic unit cells within the structure. Note that the constraint $\rho_e^{(1)} = \cdots = \rho_e^{N_\text{s}},\ e = 1, \ldots, N_e$ is prescribed to make sure the structure is composed of periodic microstructures with the existence of the RVE, which means that the pseudo densities of elements (ρ_{min} or 1 in Equation (36)) at the corresponding locations in each substructure are the same. N_e is the number of finite elements in each RVE.

During the process of evolutionary-type structural optimization, the elements are removed or added based on their sensitivity numbers. Therefore, the elements at the same locations in different substructures are removed or added simultaneously. However, the strain/stress distribution in different substructures/microscopic unit cells may not be the same in most cases. To enforce the periodic array of the microscopic unit cells, the element sensitivity numbers at the same location in each unit cell need to be consistent. They are then defined as the summation of the sensitivity of corresponding elements in all unit cells. In conventional evolutionary structural optimization method (see e.g. [15]), the element sensitivity number is defined as the change of the structural compliance or total strain energy since the removal of that element which is then equal to the elemental strain energy. Therefore, the elemental sensitivity number in this scheme can be expressed as the variation of the overall structural compliance due to the removal of $e-$th elements in all substructures:

$$\alpha_e^{cla} = \begin{cases} \sum_{k=1}^{N_s} \int_{\Omega_e^k} \boldsymbol{\sigma}^{cla}(\boldsymbol{x}) \boldsymbol{\varepsilon}^{cla}(\boldsymbol{x}) d\Omega_e^k, & \text{for } \rho_e^{(k)} = 1 \\ 0\,, & \text{for } \rho_e^{(k)} = \rho_{min}. \end{cases} \tag{37}$$

where $\boldsymbol{\sigma}^{cla}(\boldsymbol{x})$ and $\boldsymbol{\varepsilon}^{cla}(\boldsymbol{x})$ are the re-localized stress and strain fields based on the classical homogenization method. Details about computation of the re-localized stress and strain as well as the assembly of global stiffness matrix $\bar{\mathbf{K}}$ in (33) are formulated in the next section.

3.2. Finite element meshes and relocalization scheme

In order to assemble the stiffness matrix $\bar{\mathbf{K}}$ in Equation (33) at the macroscopic scale, the local problem (1)-(3) should be solved to obtain the effective material properties at the lower scale. In this scheme, a fine mesh is adopted at microscopic scale to account for all heterogeneous details within the RVE. However, coarse meshes are used to carry out the finite element analysis for macrostructure so as to save computational expense. Specific finite element meshes for both macroscopic and microscopic problems can be seen in the section of numerical examples. It is noted that the sensitivity number in Equation (37) is formulated at the finest microscopic mesh, therefore, a relocalization process is required after solving the structural problem based on coarse meshes at the higher scale to obtain the sensitivities in (37).

With the calculated effective material properties $\bar{\boldsymbol{C}}^H$ of the RVE (see Section 2), the global stiffness matrix $\bar{\mathbf{K}}$ can be assembled in a standard finite element way as:

$$\bar{\mathbf{K}} = \sum_k \int_{\Omega^k} \boldsymbol{B}^T(\boldsymbol{x}) \bar{\boldsymbol{C}}^H \boldsymbol{B}(\boldsymbol{x}) d\Omega, \tag{38}$$

where $\boldsymbol{B}$ and $\bar{\boldsymbol{C}}^H$ are the strain matrix and the effective elastic matrix within the coarse mesh element at the macro scale, respectively. With the solution of the macroscopic problem based on the coarse mesh at hand, the microscopic strain and stress fields can be reconstructed by using the localization operator in each RVE as

$$\boldsymbol{\varepsilon}^{cla}(\boldsymbol{x}) = \mathbb{A}(\boldsymbol{x}) : \bar{\varepsilon}(\bar{\mathbf{u}}(\boldsymbol{x})), \quad \forall \boldsymbol{x} \in \Omega \tag{39}$$

and

$$\boldsymbol{\sigma}^{cla}(\boldsymbol{x}) = \mathbb{C}(\boldsymbol{x}) : \mathbb{A}(\boldsymbol{x}) : \bar{\boldsymbol{\varepsilon}}(\bar{\mathbf{u}}(\boldsymbol{x})), \quad \forall \boldsymbol{x} \in \Omega \tag{40}$$

where the strain value $\bar{\varepsilon}(\bar{\mathbf{u}}(\boldsymbol{x}))$ is defined as $\bar{\varepsilon}(\bar{\mathbf{u}}(\boldsymbol{x})) = \frac{1}{2}(\nabla(\bar{\mathbf{u}}(\boldsymbol{x})) + \nabla^T(\bar{\mathbf{u}}(\boldsymbol{x})))$. The localization operator $\mathbb{A}$ has been obtained previously by solving the RVE problem (1)-(3) (see Section 2). Therefore, the sensitivity number formulated in (37) can be calculated to perform the topology optimization. We note that the sensitivity number can be naturally obtained by a reference solution when all heterogeneities are fully meshed. However, this could result in a huge amount of calculations, especially in topology optimization where the finite element analysis needs to be carried out in each iteration. In the section of examples, the optimized topologies of RVE as well as the resulted stiffness based on the presented method and on the reference solution will be compared to investigate the size effect of the RVE, with the size ranging from large to small as compared with the structure dimensions.

3.3. Optimization procedure

The BESO method starts from an initial guess of the design domain and tailors the topology according to the sensitivity numbers iteratively. In this work, the structural problem is solved on the coarse mesh to save the computational cost, and a relocalized scheme based on the classical homogenization is adopted to relocalize the microscopic fields so as to compute the sensitivity number from Equation (37). The overall optimization procedure of the topology optimization for periodic lattice microstructures using the classical homogenization scheme is formulated as follows.

1. Set both a coarse mesh and a fine mesh associated with the RVE, resulting a corresponding coarse mesh for the whole structure.
2. Assign the pseudo densities (0 *or* 1) to elements in the RVE to construct an initial design before optimization.
3. Perform the classical homogenization method on the RVE to obtain the localization tensor $\mathbb{A}$ and the effective elastic tensor $\bar{\mathbb{C}}^H$, as summarized in Section 2.
4. Solve the structure problem on the coarse mesh with the effective material property.
5. Based on the solution from the structure problem, relocalize the microscopic strain and stress fields by (39) and (40), respectively.
6. Compute the elemental sensitivity number using (37).
7. Modify the sensitivity number using a filter scheme [16] as:

$$\alpha_e = \frac{\sum_{j=1}^{N_e} w_{ej}\alpha_j}{\sum_{j=1}^{N_e} w_{ej}}, w_{ej} = \max(0, r_{\min} - \Delta(e, j)) \tag{41}$$

   where r_{min} is the filter radius which can be defined by designer, $\Delta(e, j)$ is the center-to-center distance between elements e and j. The resulted sensitivity number is further modified with its historical value to avoid big oscillations during the evolutionary process [15], i.e. $\alpha_e^{(iter)} = (\alpha_e^{(iter)} + \alpha_e^{(iter-1)})/2$. $iter$ is the current iteration number.
8. Remove inefficient materials from the RVE according to the modified sensitivity number to satisfy the volume constraint at the current iteration:

$$V_{(iter)} = \max\left\{V_{\text{req}}, (1 - c_{\text{er}})V_{(iter-1)}\right\}, \tag{42}$$

   where c_{er} is an evolutionary volume ratio which can be set by designer to determine the amount of material to be removed from the previous design iteration.
9. Repeat 3-8 until the material constraint V_{req} is satisfied and the following convergence criterion is reached:

$$\frac{|\sum_{q=1}^{Q}\left(f_{iter-q+1} - f_{iter-Q-q+1}\right)|}{\sum_{q=1}^{Q} f_{iter-q+1}} \leq \tau \tag{43}$$

   where f is the objective function, Q is the integral number and τ is a specified small value.

It is worth noted that the present homogenization method allows starting the optimization process from a homogeneous design with $\rho_e = 1$ for any e, since the microscale fields is relocalized by the nodal value on the coarse mesh of the higher scale. As a result, there is no mandatory requirement to set on or several holes for initiating the procedure which is the case in most inverse homogenization schemes for topological design of material microstructures [4, 5].

4. Numerical examples

In this section, several numerical experiments are presented to investigate the size effect of unit cell in the classical homogenization-based topology optimization of lattice/periodic structures. The dimensions of the unit cell range from large to small as compared with the dimensions of the structure in different cases. The examples consist in comparing the optimized topologies by the presented homogenization method, which is solved on the coarse mesh, with the reference solution where all heterogeneities are fully meshed. Regular meshes with 4-node elements have been adopted for all examples. Plane stress conditions are assumed. At the initiation of the topology optimization, the material distribution is homogeneous with $\rho_e = 1, \forall e$ within the RVE. The material constituting the architectural structure is assumed to be isotropic, with Young's and Poisson's coefficients given respectively by $E_m = 1000$ MPa and $\nu_m = 0.3$. During the topology optimization procedure, the interior of emerged holes is meshed with highly compliant material to maintain regular meshes, and fictitious material properties for the holes are taken as $E_i = 10^{-6}$ MPa and $\nu_i = 0.3$. The target volume fraction for the optimized topology of the RVE in all examples is 0.5.

4.1. Doubly-clamped elastic domain

In this first example, we investigate the topology optimization of periodic doubly-clamped square elastic domain as illustrated in Figure 2. The horizontal and vertical displacements of both left and right ends of the beam are fixed. A concentrated force $F = 100$ N is loaded on the centre point of this beam. The side of the square beam is $L = 1000$ mm. The structure is a lattice composed of $N_s = \eta \times \eta$ unit cells repeated periodically, with η represents the number of unit cells along each space direction. A coarse mesh composed of 5×5 elements is associated to the unit cells at the structural scale. The fine mesh on the RVE is composed of 40×40 elements to solve the local problem. 5 cases are studied: (i) $\eta = 2$; (ii) $\eta = 4$; (iii) $\eta = 8$; (iv) $\eta = 16$; (v) $\eta = 20$. These different cases correspond to the following coarse meshes for the structure: (i) 10×10 elements; (ii) 20×20 elements; (iii) 40×40 elements; (iv) 80×80 elements; and (v) 100×100 elements. The reference solution is obtained by discretizing the structure with the fine mesh for accounting for all heterogeneities, resulting into the following regular meshes for the different studied cases: (i) 80×80 elements; (ii) 160×160 elements; (iii) 320×320 elements; (iv) 640×640 elements; and (v) 800×800 elements. It is reminded that the present homogenization method allows re-localizing the microscopic fields. Then, the homogenization-based topological optimization procedure only uses the values at the nodes of the coarse mesh, reducing drastically the computational time.

Figure 3 shows the different optimized topologies of the lattice structure for several numbers of unit cells along each direction to investigate the size effect of the unit cell. Figure 3 (a) shows the final optimized geometry of the lattice obtained by the reference solution while Figure 3 (b) shows the final optimized geometry of the lattice obtained by the present homogenization method. Figure 3 (c) and (d) show the optimized geometry of one unit cell for comparison. Along rows (i) - (v), the number of unit cells repeated along each direction is increased and the ratio between the dimensions of the unit cells and the dimensions of the whole structure are decreased. We observe from Figure 3 (i) to (v) that the optimized topology converges rapidly. We can also note that even for the case (i) where the two scales can clearly not be separated, both methods lead to the same

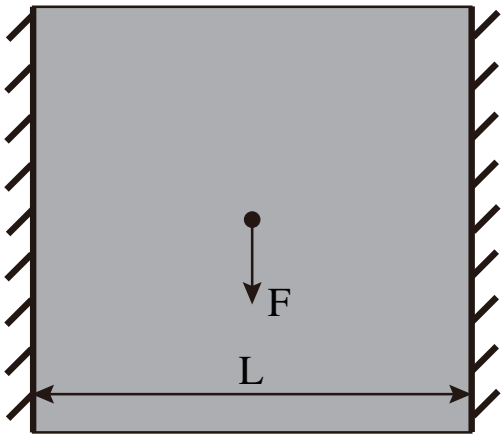

Figure 2: Doubly-clamped square elastic domain composed of periodic microscale unit cells: geometry and boundary conditions.

topology, which was not expected. To further illustrate the size effect of unit cell, we compare the compliances for optimized geometries of the lattice when using the reference solution or present homogenization-based method in Figure 4 (a). We can see that with the decrease of the unit cell size, the gap in resulted compliances is getting smaller and smaller. We also note that when the number of unit cells is large, both methods lead to the same compliance. To quantify the computational saving, the numbers of degree of freedoms (DOFs) to be solved in two different solutions are compared in Figure 4 (b). It is observed that the number of DOFs in the homogenization method is almost negligible compared with the reference solution, especially when the number of unit cells is large. Even so, the homogenization method could generate the optimized lattice structures with the same topology as well as the same stiffness as the reference solution.

4.2. L-shaped structure

In the previous example, the boundary conditions of the macrostructure were symmetrical, resulting in the optimal topological configuration of RVE being orthogonal and in a fast convergence. In this example, a more complicated L-shaped structure is investigated. The geometry of the problem is depicted in Figure 5, where the dimension of the macroscopic structure is $L = 1000$ mm. The top end of the L-shape structure is fixed, and the concentrated force is taken as $F = 100$ N (see Figure 5). The mesh used at the fine scale within the RVE is composed of 40×40 elements. A coarse mesh composed of 5×5 is associated to the unit cells at the structural scale. As in the previous example, the number of unit cells composing the beam is varied to study the size effect of the unit cell. Then, the following numbers of unit cells along each direction are investigated: (i) 2×2; (ii) 4×4; (iii) 8×8; (iv) 16×16; and (v) 20×20. Since the structure is not square, the number of unit cells in $x-$ and $y-$ directions is not the same, e.g. there are only three unit cells for the case (i). Then, the following numbers of DOFs are solved, respectively: (i) 3554; (ii) 4044; (iii) 5924; (iv) 13,284; (v) 18,764. As a comparison, the numbers of DOFs need to be solved using reference meshes are respectively: (i) 9922; (ii) 39,042; (iii) 154,882; (iv) 616,962; (v) 963,203. We can note that using the present technique, the topology optimization procedure only uses the nodal values of the coarse mesh, thus drastically reducing the computational costs.

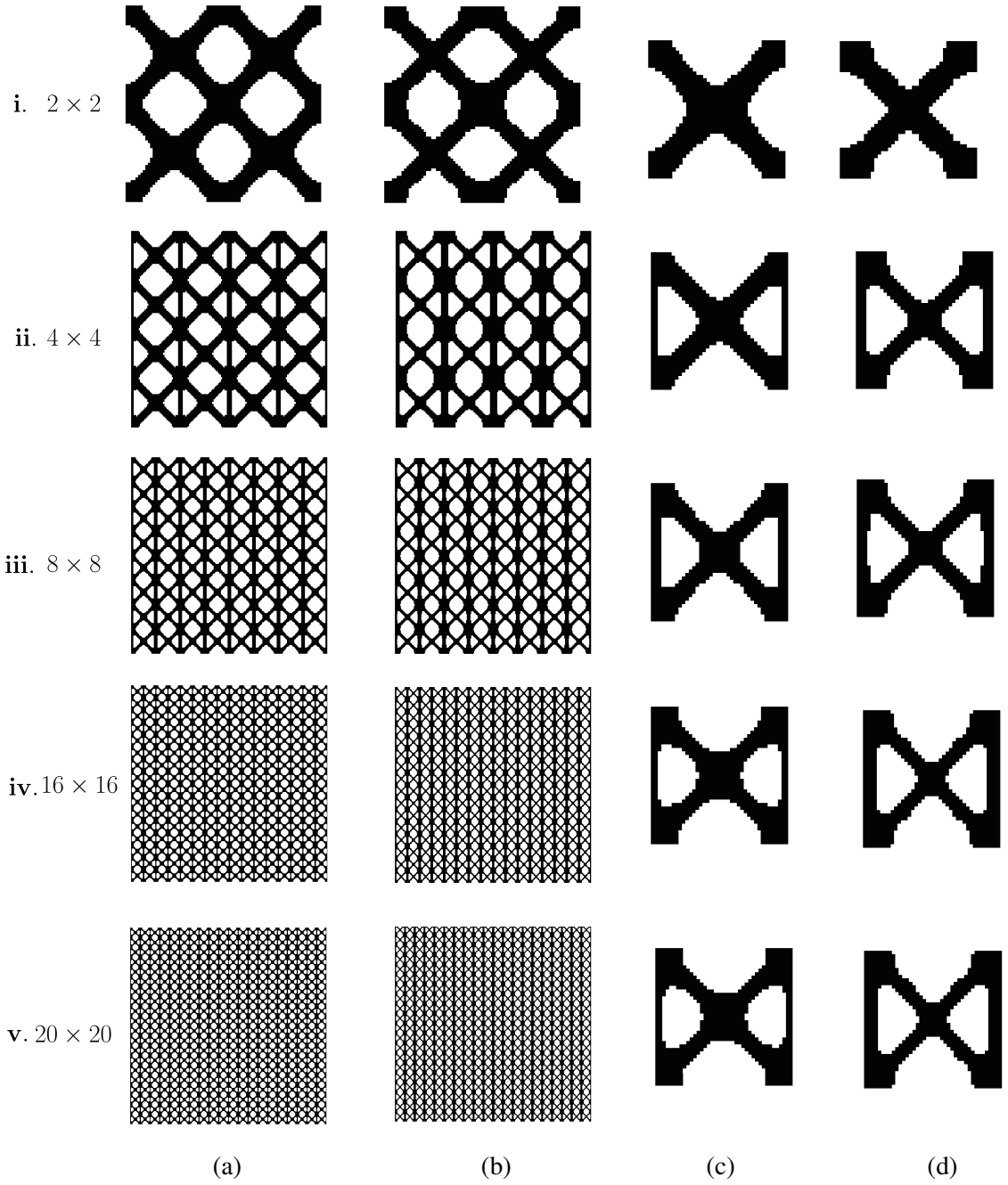

Figure 3: Optimized topologies for the double-clamped beam: columns (a), (b) compare the global lattice topologies when using the reference solution or homogenization-based method; columns (c) and (d) show the corresponding unit cell. Rows (i) to (v) correspond to increasing the number of unit cells in the lattice.

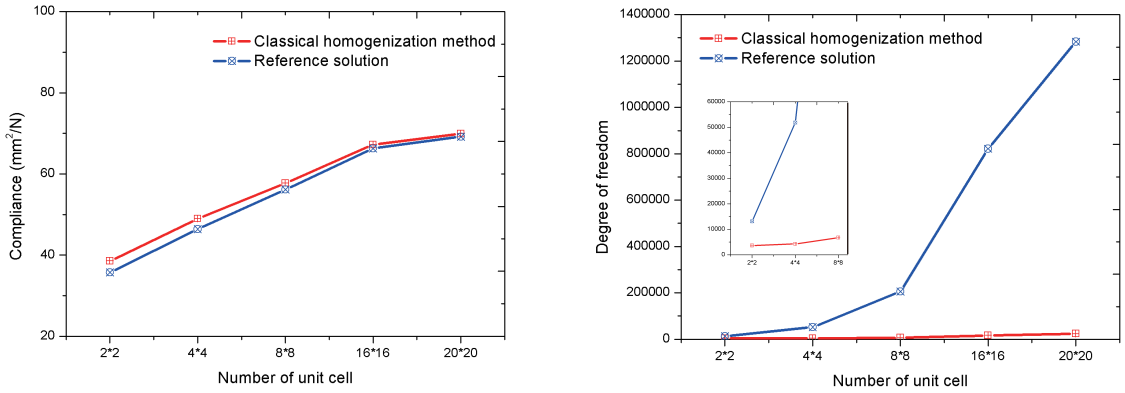

(a) (b)

Figure 4: Resulted compliance and solved DOFs by topological optimization using reference solution (blue curve) and homogenization method (red curve). Results are plotted as a function of the number of unit cells.

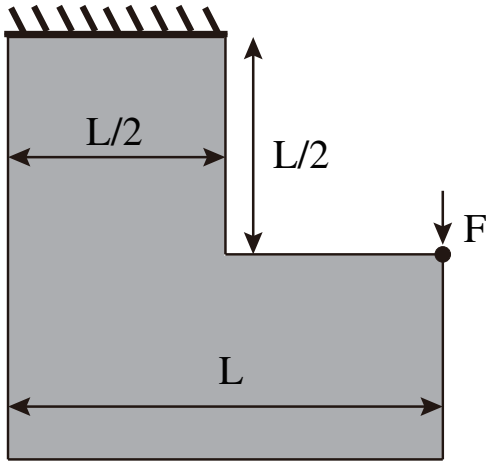

Figure 5: L-shaped beam composed of periodic microscale unit cells: geometry and boundary conditions.

As in the first example, Figure 6 shows the different optimized topologies of the lattice structure for several number of unit cells along each direction using reference solution and homogenization method. We can observe from Figures. 6 (i) and (v) that the optimized topologies have huge difference between two different solutions. However, with the large number of unit cells, the topology of optimized structure by the homogenization method is also convergent to the reference solution. We compare the compliance for the optimized geometries of the lattice using two solutions in Figure 7 (a). In this case, using the homogenization method, the obtained resulting compliance is much larger than the reference solution for the case (i). As expected, the compliance converges to the same value with the decrease of unit cell size. As an illustration, the DOFs need to be solved in two optimized models are compared in Figure 7 (b). Here again, the homogenization topology optimization method based on the coarse meshes reduces computational time significantly.

4.3. MBB beam

In this last example, we investigate the topology optimization of a periodic Messerschmitt-Bölkow-Blohm (MBB) beam subjected to a concentrated load, where the aspect ratio of the beam is chosen as 4. The geometry of the problem is depicted in Figure 8. The concentrated force load is applied at the centre of the bottom end of the domain with a magnitude $F = 100$ N. The dimensions are $L \times H = 4000 \times 1000$ mm. Since the symmetry of boundary conditions, only the right half of the MBB beam is investigated. Therefore, assuming that the half structure consists of $N_s = s_x \times s_y$ unit cells repeated periodically, with s_x and s_y denoting the number of unit cells along $x-$ and $y-$ directions, respectively. In this example, we keep $s_x = 2s_y$. 6 cases are studied: (i) $s_x \times s_y = 2 \times 1$; (ii) $s_x \times s_y = 4 \times 2$; (iii) $s_x \times s_y = 8 \times 4$; (iv) $s_x \times s_y = 16 \times 8$; (v) $s_x \times s_y = 20 \times 10$; (vi) $s_x \times s_y = 24 \times 12$. These different cases correspond to the following coarse meshes for the structure: (i) 10×5 elements; (ii) 20×10 elements; (iii) 40×20 elements; (iv) 80×40 elements; (v) 100×50 elements; (vi) 120×60 elements. As in the previous examples, the topology optimization problem of periodic structure is solved using the reference mesh (fully accounting for the heterogeneities). In the reference model, the different cases have the following fine meshes for the structure: (i) 80×40 elements; (ii) 160×80 elements; (iii) 320×160 elements; (iv) 620×320 elements; (v) 800×400 elements; (vi) 960×480 elements, respectively.

Figure 9 shows the different optimized topologies of the lattice structure for several number of unit cells along each direction, using the homogenization-based and reference methods. Here again, the optimized topologies are different in the first few cases, while both methods lead to the same topology with the large number of unit cells. We also compare the compliances for optimized geometries of the lattice using the homogenization-based and reference solutions. It is observed that obtained resulting compliance using classical homogenization is much larger than reference solution for the case (i) where the scales can clearly not be separated. However, as expected, both methods lead to the same value of the compliance when the number of unit cell in short side is larger than 8. We also compare the DOFs solved in two methods in Figure 10. It is then suggested that the present classical homogenization method can be chosen for topology optimization of periodic structures with large number of unit cells.

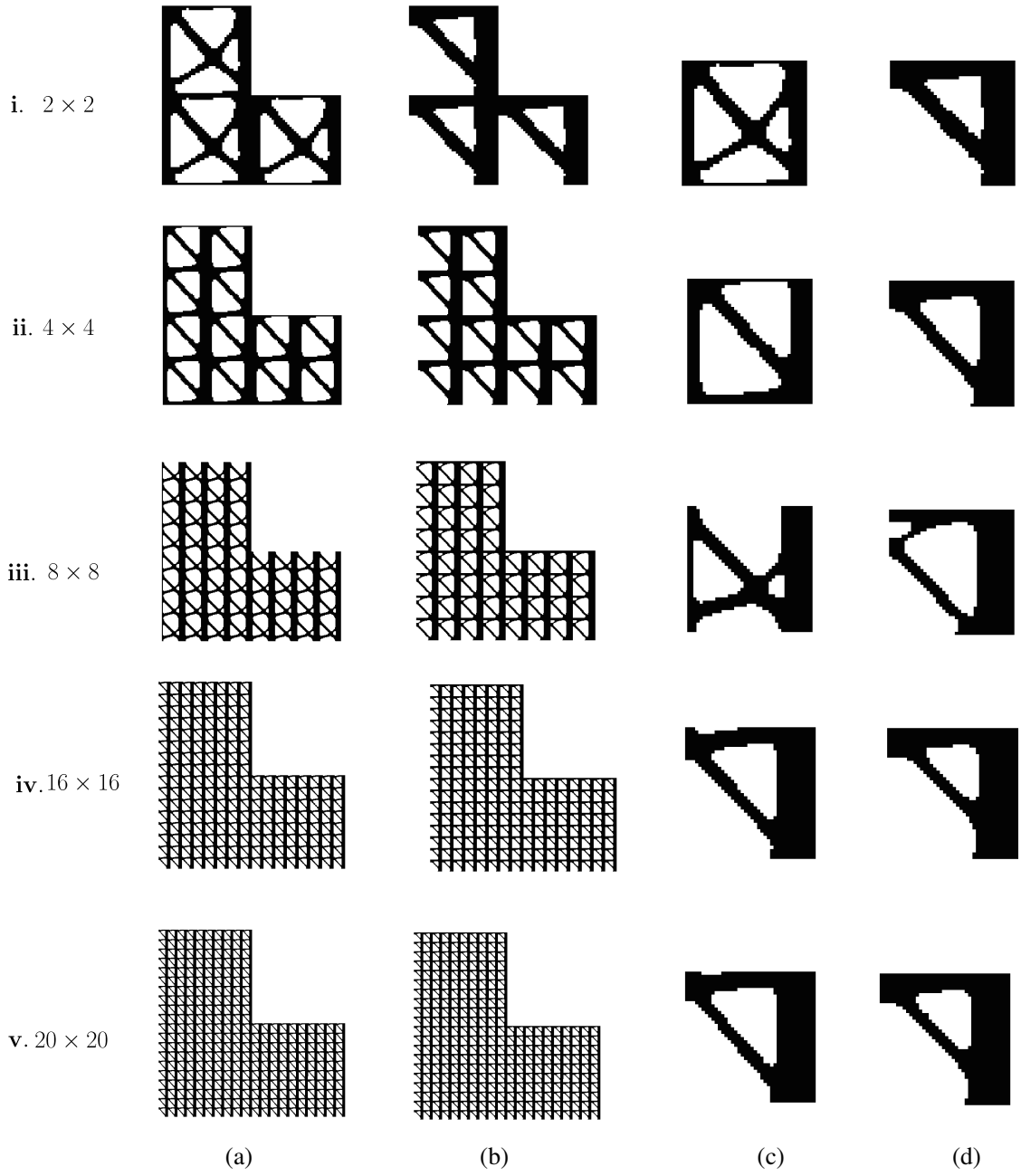

Figure 6: Optimized topologies for the L-shaped beam: columns (a), (b) compare the global lattices topologies when using the reference solution or homogenization-based method; columns (c) and (d) show the corresponding unit cell. Rows (i) to (v) correspond to increasing the number of unit cells in the lattice.

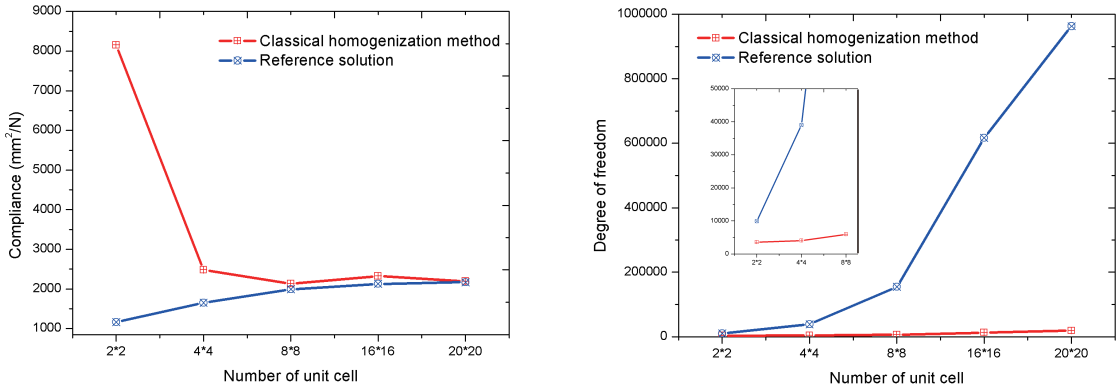

(a) (b)

Figure 7: Resulted compliance and solved DOFs by topological optimization using reference solution (blue curve) and homogenization method (red curve). Results are plotted as a function of the number of unit cells.

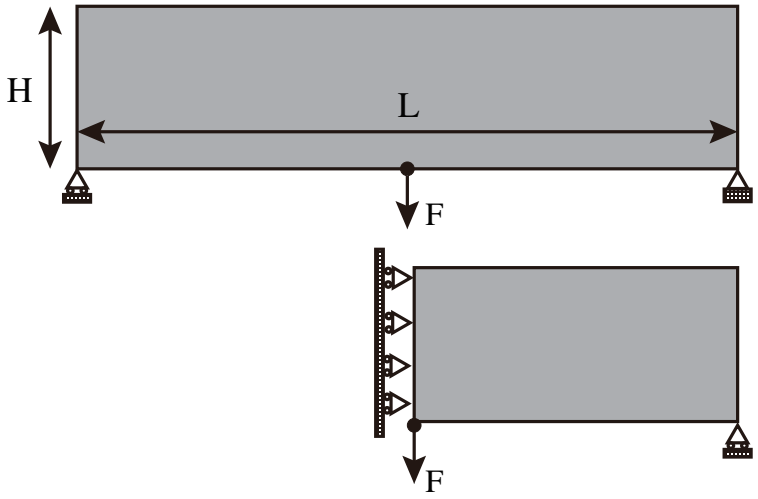

Figure 8: MBB beam composed of periodic microscale unit cells: geometry and boundary conditions.

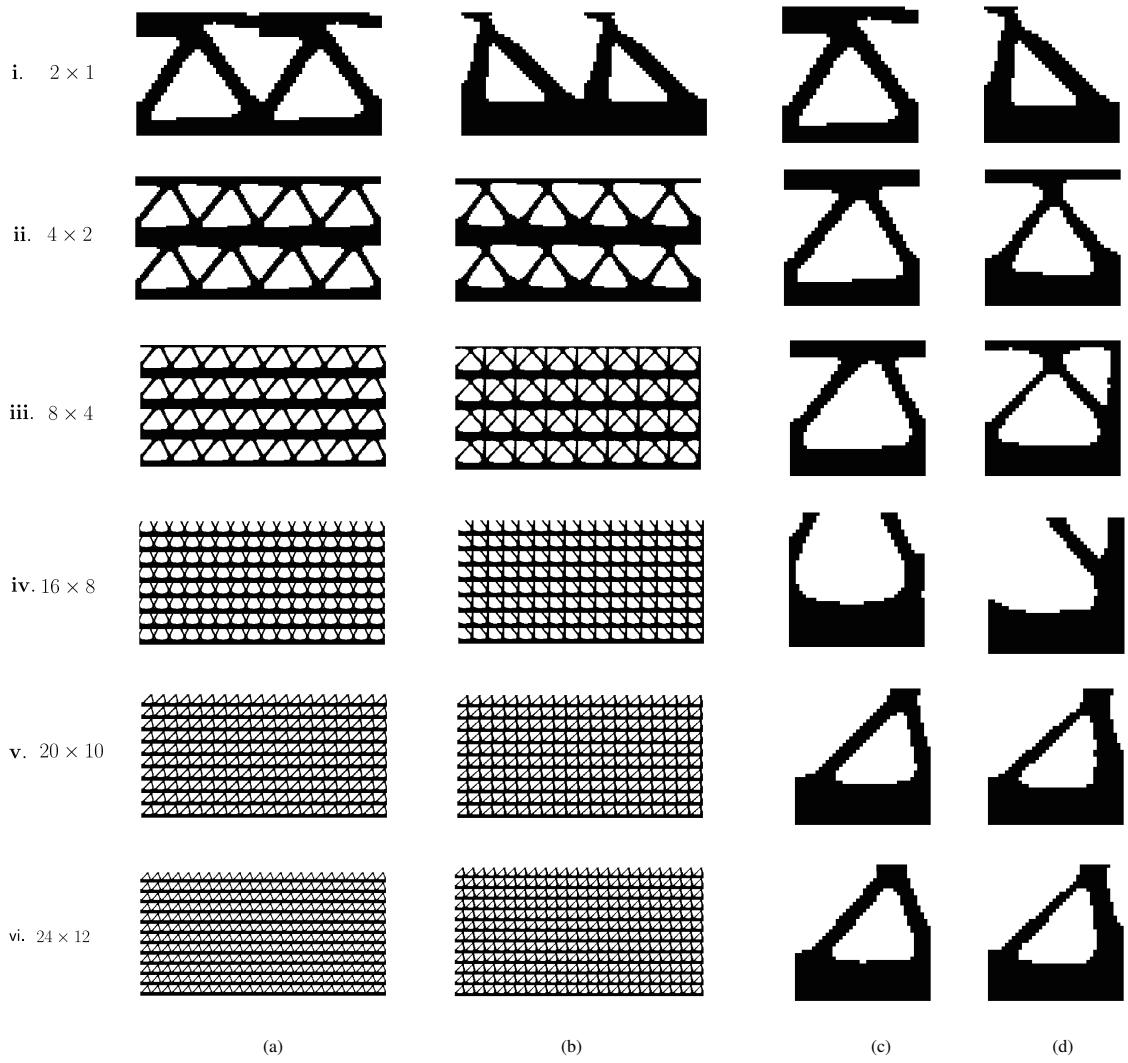

Figure 9: Optimized topologies for the half MBB beam: columns (a), (b) compare the global lattice topologies when using the reference solution and homogenization-based method; columns (c) and (d) show the corresponding unit cell. Rows (i) to (v) correspond to increasing the number of unit cells in the lattice.

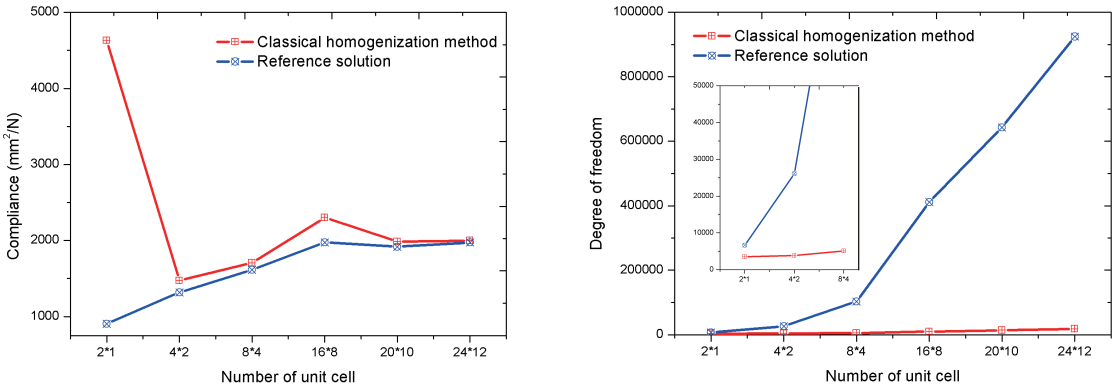

(a) (b)

Figure 10: Resulted compliance and number of DOFs using reference solution (blue curve) and homogenization method (red curve). Results are plotted as a function of the number of unit cells.

5. Conclusions

This paper presents a topology optimization of periodic structures based on the classical homogenization method by abandoning the scale separation hypothesis, i.e. the characteristic dimensions of the periodic unit cells in the lattice are comparable with the dimensions of the whole structure. The present method uses a coarse mesh corresponding to a homogenized medium based on the classical numerical homogenization, allowing reducing the micro fields to perform the topology optimization. On the other hand, topology optimization using a fully detailed description of the heterogeneous structure is performed as a comparison. Size effect of the periodic unit cell is investigated to analysis the effectiveness of the present topology optimization based on classical homogenization method. We have shown that the present topology optimization will lead to optimized structure with higher compliance when the scales can clearly not be separated (few numbers of unit cells). Furthermore, with the increase of number of unit cells, the number of degrees of freedom to be solved can be drastically reduced as compared with the reference solution. In other words, for a large number of unit cells, the present method takes less time to obtain the optimized lattice structure without losing any stiffness.

Acknowledgements

References

[1] J. C. Michel, H. Moulinec, P. Suquet, Effective properties of composite materials with periodic microstructure: A computational approach, Computer Methods in Applied Mechanics and Engineering 172 (1-4) (1999) 109–143.

[2] M. P. Bendsoe, N. Kikuchi, Generating optimal topologies in structural design using a homogenization method, Computer Methods in Applied Mechanics and Engineering 71 (2) (1988) 197–224.

[3] O. Sigmund, Materials with prescribed constitutive parameters: An inverse homogenization problem, International Journal of Solids and Structures 31 (17) (1994) 2313–2329.

[4] O. Sigmund, S. Torquato, Design of materials with extreme thermal expansion using a three-phase topology optimization method, Journal of the Mechanics and Physics of Solids 45 (6) (1997) 1037–1067.

[5] L. Xia, P. Breitkopf, Design of of materials using topology optimization and energy-based homogenization approach in matlab, Structural and Multidisciplinary Optimization 52 (6) (2015b) 1229–1241.

[6] D. C. Da, J. H. Chen, X. Y. Cui, G. Y. Li, Design of materials using hybrid cellular automata, Structural and Multidisciplinary Optimizationdoi:10.1007/s00158-017-1652-1.
[7] Y. Wang, Z. Luo, N. Zhang, Z. Kang, Topological shape optimization of microstructural metamaterials using a level set method, Computational Materials Science 87 (2014) 178–186.
[8] Y. M. Xie, X. Yang, J. Shen, X. Yan, A. Ghaedizadeh, J. Rong, X. Huang, S. Zhou, Designing orthotropic materials for negative or zero compressibility, International Journal of Solids and Structures 51 (23-24) (2014) 4038–4051.
[9] A. Clausen, F. Wang, J. S. Jensen, O. Sigmund, J. A. Lewis, Topology optimized architectures with programmable poisson's ratio over large deformations, Advanced Materials 27 (37) (2015) 5523–5527.
[10] Y. Noguchi, T. Yamada, K. Izui, S. Nishiwaki, Optimum design of an acoustic metamaterial with negative bulk modulus in an acoustic-elastic coupled system using a level set–based topology optimization method, International Journal for Numerical Methods in Engineering 113 (8) (2018) 1300–1339.
[11] G. Dai, W. Zhang, Size effects of basic cell in static analysis of sandwich beams, International Journal of Solids and Structures 45 (9) (2008) 2512–2533.
[12] C. Czech, P. Guarneri, J. Gibert, G. Fadel, On the accurate analysis of linear elastic meta-material properties for use in design optimization problems, Composites Science and Technology 72 (5) (2012) 580–586.
[13] P. Coelho, L. Amiano, J. Guedes, H. Rodrigues, Scale-size effects analysis of optimal periodic material microstructures designed by the inverse homogenization method, Computers & Structures 174 (2016) 21–32.
[14] J. Yvonnet, Computational Homogenization of Heterogeneous Materials with Finite Elements, Springer, 2019.
[15] X. Huang, Y. M. Xie, Convergent and mesh-independent solutions for the bi-directional evolutionary structural optimization method, Finite Elements in Analysis and Design 43 (14) (2007) 1039–1049.
[16] O. Sigmund, A 99 line topology optimization code written in matlab, Structural and Multidisciplinary Optimization 21 (2) (2001) 120–127.